Volume 12
Number 24
28 June 2024
Pages 8573–8988

Journal of Materials Chemistry C

Materials for optical, magnetic and electronic devices

rsc.li/materials-c

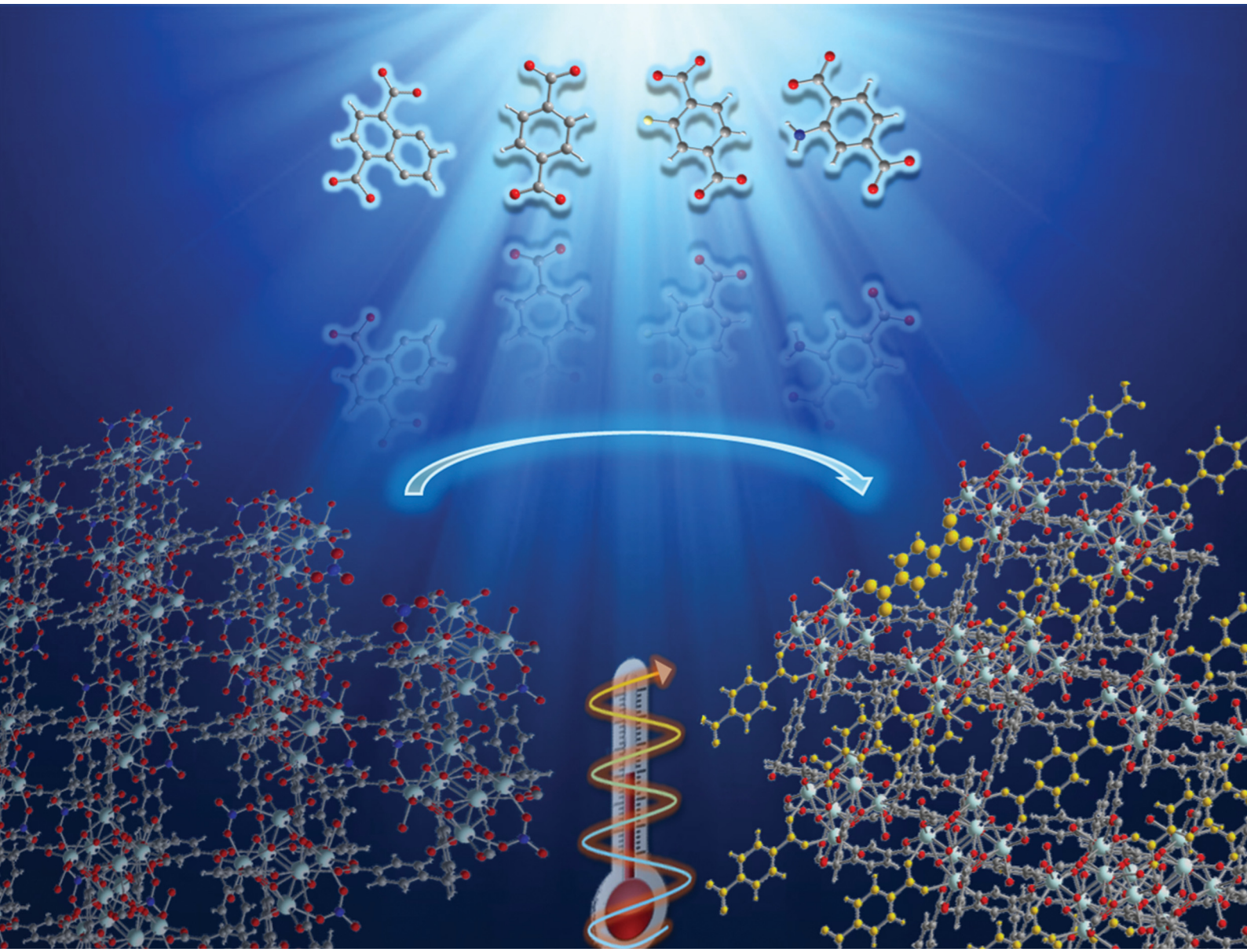

ISSN 2050-7526

ROYAL SOCIETY OF CHEMISTRY

PAPER

Hélène Serier-Brault, Anastasios J. Tasiopoulos *et al.*
Linker installation transformations in a 2-D rare earth MOF: increase of the dimensionality and turn on of the temperature sensing capability

Journal of Materials Chemistry C

ROYAL SOCIETY OF CHEMISTRY

PAPER

View Article Online
View Journal | View Issue

Cite this: J. Mater. Chem. C, 2024, 12, 8684

Linker installation transformations in a 2-D rare earth MOF: increase of the dimensionality and turn on of the temperature sensing capability†

Laoura K. Komodiki,[a] Nikos Panagiotou,[a] Hélène Serier-Brault *[b] and Anastasios J. Tasiopoulos *[a]

A new family of 2-D 8-connected rare earth (RE) MOFs based on a hexanuclear $(RE^{3+})_6$ secondary building unit (SBU), the increase of the dimensionality through single-crystal-to-single-crystal (SCSC) linker installation reactions and the turn-on of the temperature sensing capability upon these reactions are reported. The reaction of $RE(NO_3)_3$ with 4,4′-(hydroxymethylene)dibenzoic acid (H_2BCPM) in the presence of 2-fluorobenzoic acid (HFBA) in DMF/H_2O at 115 °C afforded compounds $[RE_6(\mu_3\text{-}OH^-/F^-)_8(BCPM)_4(NO_3)_2(H_2O)_4]_n$ (**UCY-17**(RE); RE: Y, Gd, Tb, Dy, Ho, Er) which represent rare examples of 2D 8-c MOFs based on a hexanuclear $(RE^{3+})_6$ SBU. The excellent quality of single crystals of **UCY-17**(Tb) and the distance between the terminal nitrate ions prompted us to investigate the SCSC exchange of NO_3^- anions by various dicarboxylate ligands aiming to bridge adjacent 2D nanosheets and form 3-D analogues. These SCSC linker installation reactions afforded a series of 3-D, 10-connected mixed linker MOFs with the general formulae $[RE_6(\mu_3\text{-}OH^-/F^-)_8(BCPM)_4(L)(H_2O)_4]_n$ (**UCY-17**(Tb)/L; H_2L = H_2BDC (1,4-benzenedicarboxylic acid), H_2ABDC (2-aminobenzene-1,4-dicarboxylic acid), H_2FBDC (2-fluorobenzene-1,4-dicarboxylic acid), and H_2NDC (1,4-naphthalenedicarboxylic acid)). The exchanged analogues of **UCY-17**(Gd) and **UCY-17**($Eu_{0.05}Tb_{0.95}$) were synthesized and the thermometric properties of the latter were investigated. These studies revealed that there is no thermal evolution of the emission properties for the pristine MOF **UCY-17**($Eu_{0.05}Tb_{0.95}$) whereas the exchanged analogues exhibit significant thermometric properties at higher temperatures (>270 K). The maximum thermal sensitivity of most exchanged derivatives appears at physiological temperatures and ranges between 300 and 355 K. Overall, this work proposes a promising strategy for increasing the dimensionality of 2-D MOFs and controlling the thermometric performances of mixed $Eu_{0.05}Tb_{0.95}$ MOFs.

Received 12th March 2024,
Accepted 26th April 2024

DOI: 10.1039/d4tc00992d

rsc.li/materials-c

Introduction

Metal–organic frameworks, referred to as MOFs, are a class of porous materials that have attracted tremendous research interest[1] due to their significant potential for practical applications in different areas such as gas storage and separation,[2–4] drug delivery,[5] sensing,[6–9] and catalysis.[10,11] This stems from the fact that MOFs exhibit microporous structures with large surface areas and tunable functionalities, pore sizes and topologies.[12] A wide range of different metal ions or preformed metal clusters and organic ligands (with or without functional groups) can be utilised for the synthesis of MOFs depending on the targeted application.[13] Thus, MOFs with different network topologies and structural properties can be easily designed and synthesized, giving rise to materials with a wide range of different metal ions, organic ligands, secondary building units (SBUs), functional groups, network topologies, *etc.*, by employing principles of the molecular building block (MBB) approach.[14,15]

An important evolvement of MOF chemistry was the synthesis of a Zr^{4+} MOF based on a hexanuclear $[Zr_6(\mu_3\text{-}O)_4(\mu_3\text{-}OH)_4]^{12+}$ SBU, known as UiO-66,[16] which opened up several new research directions in the field. This is because UiO-66 exhibits significant thermal, chemical and hydrolytic stability.[17] One of the research goals in this area involved the synthesis of analogous compounds based on a hexanuclear SBU with different metal ions, which led to a series of RE^{3+},[18] Ce^{4+},[19] U^{4+}[20] and Th^{4+}[19,20] MOFs. Among them, MOFs based on polynuclear SBUs with

[a] Department of Chemistry, University of Cyprus, 1678 Nicosia, Cyprus. E-mail: atasio@ucy.ac.cy
[b] Nantes Université CNRS Institut des Matériaux de Nantes Jean Rouxel, IMN Nantes F-44000, France. E-mail: helene.brault@cnrs-imn.fr

† Electronic supplementary information (ESI) available: Experimental details and figures/tables related to the structural and physicochemical characterisation of the reported compounds. CCDC 2338720–2338729. For ESI and crystallographic data in CIF or other electronic format see DOI: https://doi.org/10.1039/d4tc00992d

RE^{3+} ions, have attracted attention because of their increased thermal/chemical/hydrolytic stability and their interesting photoluminescence[21] and magnetic[22] properties. Our group is active in this field and we recently reported a family of 8-connected 2-D MOFs based on a hexanuclear SBU and 4,4′-sulfonyldibenzoic acid (H_2SDBA) ligand with capability to selectively detect gases of selected volatile and nitroaromatic organic compounds.[23]

Another important synthetic method in the field of MOFs is post synthesis modification (PSM) which includes the modification of the structure of a MOF after it has been synthesized. It is preferable for PSM to proceed in a single-crystal-to-single-crystal (SCSC) fashion because in this way direct structural information can be provided for the achieved structural alterations through single crystal X-ray crystallography. Several types of SCSC transformations have been reported[24] which include insertion/exchange of organic ligands,[25] exchange of lattice solvent molecules or terminally ligated molecules,[26–28] transmetallation,[29] metalation of frameworks,[30] *etc.* The main goal in this field is the improvement or fine-tuning of the magnetic,[30–32] catalytic,[33,34] sorption,[35] photoluminescence[36] and sensing[37] properties as well as the elucidation of the exact mechanisms of these processes that could potentially enable further optimization to be achieved. RE-MOFs have been ideal targets for SCSC reactions since their photoluminescence, magnetic and sensing properties can be directly monitored and fine-tuned. Solvent assisted linker installation (SLI) reactions that proceed in an SCSC fashion involving the replacement of terminally ligated solvent molecules or anions by bridging ligands have led to tailored MOFs with specific pore sizes and internal functional groups and properties.[25,34,38,39] Such SCSC transformations have taken place in Zr^{4+} and in polynuclear RE^{3+} MOFs, leading to the installation of various dicarboxylic ligands and also in the improvement of the thermal stability,[40] catalytic[34] and gas sorption[35] properties. These examples included the transformation of an 8-connected 3-D Zr^{4+} MOF to 10-, 11- and 12-connected 3-D MOFs[34,35,38] and a 6-connected 2-D Y^{3+} MOF to a 12-connected 3-D one.[40]

Another property that could be modulated through SCSC transformations of RE^{3+} MOFs is their temperature sensing capability which is based on the photoluminescence response of lanthanide ions (and organic ligands).[41] Significant attention in this field is focused on Eu–Tb MOF luminescent thermometers, which take advantage of the unique luminescence properties of the constituent metal ions for accurate and responsive temperature measurements. Rare earth ions (RE^{3+}) exhibit distinctive luminescence behaviours that change with temperature, allowing them to serve as the basis for luminescence-based temperature sensors. The advantages of using RE-MOFs as thermometers include their high sensitivity, reversible response, and potential for remote sensing using luminescence signals.[42] Despite the fact that there are quite a few mixed metal RE^{3+} MOFs, mainly Eu–Tb ones, that have been studied as temperature sensors[43–45] the list of hexanuclear $(RE^{3+})_6$ MOFs investigated as photoluminescence thermometers is quite limited.[46,47] In addition, there are very few studies investigating the fine tuning of the thermometry properties of MOFs through SCSC transformations. We recently reported on the modulation of the thermometry properties of a mixed metal $Eu_{0.05}Tb_{0.95}$-ABDC (H_2ABDC (2-aminobenzene-1,4-dicarboxylic acid)) MOF through the replacement of the terminally ligated DMF molecules by various terminal or chelating organic ligands which led to a shift of 50 K of the operating temperature range of the exchanged analogues compared to the one of the pristine compound.[48] Additional investigations in this field involved a PSM that led to the turn on of the photoluminescence and the temperature sensing capability of a non-luminescent pristine material[49] and the study of the thermometric properties of an Eu^{3+} MOF and its guest as well as the guest and coordinated solvent molecules exchanged analogues.[50] However, there are no studies involving the investigation of the role of bridging ligands on the photophysical and/or temperature sensing properties by employing the PSM method. To achieve this, post synthesis modifications should be realized in which the insertion of simple polytopic ligands as 1,4-benzenedicarboxylic acid (H_2BDC) and its derivatives would be the main structural alteration; other important structural features of the MOF including coordination number/coordination geometry of the metal ions or number and coordination modes of the existing ligands, *etc* should remain essentially unaffected upon these reactions.

We herein report the synthesis and characterization of a new family of 8-connected 2-D MOFs based on a hexanuclear $(RE^{3+})_6$ SBU and the angular dicarboxylic acid ligand 4,4′-(hydroxymethylene)dibenzoic acid (H_2BCPM) with the general formula $[RE_6(\mu_3\text{-}OH^-/F^-)_8(BCPM)_4(NO_3)_2(H_2O)_4]_n$ (**UCY-17**(RE); RE: Y, Gd, Tb, Dy, Ho, and Er) and the exchanged analogues produced from linker installation SCSC reactions of **UCY-17**(Tb) with selected dicarboxylic ligands. Interestingly, compounds $[RE_6(\mu_3\text{-}OH/F)_8(BCPM)_4(L)(H_2O)_4]_n$ (**UCY-17**(RE)/L; RE = Gd, Tb, H_2L = H_2BDC (1,4 benzenedicarboxylic acid), H_2ABDC (2-aminobenzene-1,4-dicarboxylic acid), H_2FBDC (2-fluorobenzene-1,4-dicarboxylic acid), H_2NDC (1,4-naphthalenedicarboxylic acid)) represent rare examples of 10-connected 3-D MOFs containing polynuclear SBUs. Detailed photophysical studies revealed that the installation of a second linker in the **UCY-17**($Eu_{0.05}Tb_{0.95}$) bimetallic analogues has a significant effect on the sensitization efficiency of the Tb^{3+} and Eu^{3+} ions. In fact, the SCSC installation of these dicarboxylic ligands results not only in the turn-on of the thermometric properties of this family of materials but also in a variety of different thermometric performances. Overall, the SCSC linker installation process in compound **UCY-17**(RE) led not only to significant structural variations, including the increase of its dimensionality and the formation of analogous compounds with uncommon structural features but also to materials displaying a variety of photoluminescence and thermometric properties.

Experimental

Materials

Reagent grade chemicals and solvents (analytical grade) were purchased from commercial sources (Aldrich, Merck, Alfa

Aesar, TCI, BLD-pharm, *etc*) and used without further purification. All synthetic procedures were carried out in the air. 4,4′-carbonyldibenzoic acid, 2-fluorobenzene-1,4-dicarboxylic acid, 1,4-naphthalenedicarboxylic acid were purchased from BLD-pharm and 1,4 benzenedicarboxylic acid, 2-aminobenzene-1,4-dicarboxylic acid and 2-fluorobenzoic acid (HFBA) from Sigma-Aldrich. 4,4′-(Hydroxymethylene)dibenzoic acid was synthesized following a procedure reported in the literature.[51]

Synthesis

Synthesis of **UCY-17**(RE) (RE: Y, Gd, Tb, Dy, Ho, Er). Solid $RE(NO_3)_3{\cdot}xH_2O$ (x = 5 or 6) (0.2 mmol) was added in one portion to a clear solution of H_2BCPM (0.14 g, 0.5 mmol), and HFBA (0.20 g, 1.4 mmol) in DMF: H_2O (4 ml : 1 ml) in a 20 ml glass vial and sonicated until complete dissolution of the reactants. The vial was sealed, placed in an oven at 115 °C and left undisturbed for 6 days. Then it was cooled to room temperature and colourless rhombic plate crystals of **UCY-17**(RE) were isolated by filtration, washed with DMF (3 × 4 ml) and dried in air. The reaction yields were in the range of 60–65% based on H_2BCPM. Anal. calcd **UCY-17**(Y)·16DMF ($Y_6O_{54}N_{18}C_{108}H_{168}$): C 41.63; H 5.43; N 8.09; found: C 41.40; H 5.64; N 8.28. **UCY-17**(Gd)·17DMF ($Gd_6O_{55}N_{19}C_{111}H_{175}$): C 37.04; H 4.90; N 7.39; found: C 37.26; H 4.78; N 7.60. **UCY-17** (Tb)·16DMF ($Tb_6O_{54}N_{18}C_{108}H_{168}$): C 36.68; H 4.79; N 7.13; found: C 36.96; H 4.91; N 7.25. **UCY-17**(Dy)·15DMF ($Dy_6O_{53}N_{17}C_{105}H_{161}$): C 36.19; H 4.66; N 6.83; found: C 36.35; H 4.88; N 6.95. **UCY-17**(Ho)·17DMF ($Ho_6O_{55}N_{19}C_{111}H_{175}$): C 36.57; H 4.84; N 7.30; found: C 36.79; H 4.67; N 7.06. **UCY-17**(Er)·17DMF ($Er_6O_{55}N_{19}C_{111}H_{175}$): C 36.43; H 4.82; N 7.27; found: C 36.18; H 4.95; N 7.48.

Synthesis of **UCY-17**($Eu_{0.05}Tb_{0.95}$). Solutions (0.1 M) of $Eu(NO_3)_3{\cdot}5H_2O$ (0.5 ml, 0.05 mmol) and $Tb(NO_3)_3{\cdot}5H_2O$ (9.5 ml, 0.95mmol) in DMF were added to a clear solution of H_2BCPM (0.68 g, 2.5 mmol) and HFBA (1.0 g, 7.1 mmol) in DMF: H_2O (20 ml : 5 ml) in a 50 ml glass vial. The vial was sealed, placed in an oven at 115 °C and left undisturbed for ∼5 days. Then it was cooled to room temperature and colourless rhombic plate crystals of **UCY-17**($Eu_{0.05}Tb_{0.95}$) were isolated by filtration, washed with DMF (3 × 20 ml) and dried in air. The yield was 60% based on H_2BCPM. The metal ion content was determined by inductively coupled plasma atomic emission spectrometry (ICP-AES) and provided a Tb^{3+}/Eu^{3+} ratio of 0.937/0.063.

Synthesis of **UCY-17**(RE)/L (RE: Gd, Tb, $Eu_{0.05}Tb_{0.95}$, H_2L = H_2BDC = 1,4 benzenedicarboxylic acid, H_2ABDC = 2-aminobenzene-1,4-dicarboxylic acid, H_2NDC = 1,4-naphthalenedicarboxylic acid, and H_2FBDC = 2-fluorobenzene-1,4-dicarboxylic acid). Single crystals of as synthesized **UCY-17**(RE) (50 mg) were added to a solution of the desired ligand in DMF (20 ml, 25 mM, 0.5 mmol) in a 50 ml glass vial. The vial was sealed, placed in an oven at 80 °C and left undisturbed for 4 days. Then it was cooled to room temperature, the solvent was decanted and the single crystals of **UCY-17**(RE)/L were washed with hot (at 80 °C) DMF (20 ml) once a day for 5 days. The crystals were collected by filtration and dried in air. Anal. calcd **UCY-17**(Tb)/BDC·22DMF ($Tb_6O_{58}N_{22}C_{134}H_{214}$): C 40.09; H 5.37 N 7.68; found: C 40.41; H 5.60; N 7.88. **UCY-17**(Tb)/ABDC·20DMF ($Tb_6O_{56}N_{21}C_{128}H_{201}$): C 39.59; H 5.22 N 7.57; found: C 39.30; H 5.05; N 7.35. **UCY-17**(Tb)/FBDC·11DMF ($Tb_6F_1O_{47}N_{11}C_{101}H_{136}$): C 37.57; H 4.25; N 4.77; found: C 37.83; H 4.44; N 4.90. **UCY-17**(Tb)/NDC·19DMF ($Tb_6O_{55}N_{19}C_{129}H_{195}$) C 40.29; H 5.11 N 6.92; found: C 40.05; H 4.86; N 6.71. ICP-AES studies for **UCY-17**($Eu_{0.05}Tb_{0.95}$)/L exchanged analogues provided Tb^{3+}/Eu^{3+} ratio within the range 0.942/0.058 – 0.936/0.064; the exact ratios of all exchanged analogues are reported in Table S1 in the ESI.†

Physical measurements

Elemental analyses (C, H, and N) were performed using the in-house facilities of the University of Cyprus, Chemistry Department. IR spectra were recorded on ATR in the 4000–700 cm^{-1} range using a Shimadzu Prestige – 21 spectrometer. PXRD patterns were recorded on a Rigaku MiniFlex 6G X-ray diffractometer (Cu Kα radiation, λ = 1.5418 Å) equipped with a D/teX Ultra 1D silicon strip X-ray detector. Thermal stability studies were performed with a Shimadzu TGA 50 thermogravimetric analyzer. ^{1}H NMR spectra were recorded on a Bruker Avance III 300 MHz spectrometer at 25 °C. Chemical shift values in ^{1}H NMR and ^{19}F NMR spectra were reported in parts per million (ppm). Digestion of the samples (∼10 mg) was achieved with 0.5 M KOH in D_2O or with 25 μL of concentrated DCl in d_6-DMSO.

Stability studies at a certain temperature

The stability of compounds **UCY-17**($Eu_{0.05}Tb_{0.95}$) and **UCY-17**($Eu_{0.05}Tb_{0.95}$)/L at 90 °C was studied as follows: ∼50 mg of a microcrystalline sample of a given compound was added to a glass vial which was placed in an oven operating at 90 °C and left undisturbed for 30 minutes. Then the temperature of the oven was slowly decreased until it reached room temperature and the pXRD patterns of the microcrystalline samples were recorded.

Photophysical studies

Solid-state photoluminescence measurements (emission, excitation and lifetimes) were recorded at room temperature on a Jobin Yvon Fluorolog 3 spectrofluorometer equipped with a CCD camera (excitation source: 450 W Xe arc lamp) and a JASCO FP-8300 spectrofluorometer. The emission spectra were corrected for detection and optical spectral response of the spectrofluorometer, and the excitation spectra were weighed for the spectral distribution of the lamp intensity using a photodiode reference detector. The low temperature measurements were performed on a Jobin Yvon spectrofluorometer in a front-face configuration. The excitation spectra were corrected for the variation of the incident flux (450W Xe lamp); the emission spectra were corrected for the transmission of the monochromator as well as the response of the photomultiplier. Slit apertures, increments, and acquisition times were adjusted for optimized signal-to-noise ratio and resolution. An Oxford cryostat connected to a dynamic pumping system ensured the circulation of nitrogen gas. The temperature was monitored through a thermal probe in direct contact with the copper

sample holder. After reaching the targeted temperature, a dwell time of 10 minutes was fixed before launching the emission/excitation acquisition to ensure the thermal homogeneity of the sample.

Single crystal X-ray crystallography

Single crystal X-ray diffraction data were collected on a Rigaku Supernova A diffractometer, equipped with a CCD area detector and a Rigaku Synergy S X-ray diffractometer, equipped with an HyPix-6000HE area detector utilizing Cu-Kα (λ = 1.5418 Å) radiation. A suitable crystal was mounted on a Hampton cryoloop with paratone-N oil and transferred to a goniostat where it was cooled for data collection. The structures were solved by direct methods using SHELXT and OLEX2[52] and refined on F^2 using full-matrix least squares with SHELXL14.1.[53] Software packages used were as follows: CrysAlis CCD for data collection, CrysAlis RED for cell refinement and data reduction,[54] WINGX for geometric calculations,[55] and DIAMOND for molecular graphics.[56] The non-H atoms were treated anisotropically, whereas the aromatic hydrogen atoms were placed in calculated, ideal positions and refined as riding on their respective carbon atoms. Several restraints (DFIX, SIMU, RIGU and DELU) were used to fix the thermal ellipsoids and geometry of the NO_3^- ions, the –OH group and phenyl rings of the $BCPM^{2-}$ ligand and the phenyl rings of the NDC^{2-} anion. Electron density contributions from disordered guest molecules were handled using the SQUEEZE procedure from the PLATON software suit[57] due to the disordered nature of these molecules. Selected crystal data for **UCY-17**(RE) (RE: Y, Gd, Tb, Dy, Ho, and Er) and the exchanged analogues **UCY-17**(Tb)/L (L = BDC^{2-}, $ABDC^{2-}$, $FBDC^{2-}$ and NDC^{2-}) are summarized in Tables S2 and S3, respectively, in the ESI.† CCDC 2338720–2338729 contain the supplementary crystallographic data for this paper. Full details can be found in the CIF files provided in the ESI.†

Results and discussion

Synthesis and structural characterization

The research group of one of us has recently focused on the synthesis of chemically stable Zr^{4+} or RE^{3+} MOFs based on hexanuclear SBUs with angular dicarboxylic ligands. We successfully isolated two 2D 8-c $(Zr^{4+})_6$ MOFs, **UCY-13** and **UCY-14** with the ligands H_2HFPBBA (4,4′-(hexafluoroisopropylidene)-bis(benzoic acid)) and H_2OBA (4,4′-Oxybis(benzoic acid)) which are stable in aqueous solutions and exhibit exceptional UO_2^{2+} sorption capacity.[58] Furthermore, the angular dicarboxylic acid H_2OBA afforded a series of 12-c anionic RE-pcu-MOFs (RE: Y, Tb, Dy, Ho).[59] Also, a new family of 2D-8c-RE-MOFs, **UCY-15**(RE) (RE: Y, Eu, Gd, Tb, Dy, Ho, Er), analogous to **UCY-13** was reported with the angular dicarboxylic ligand H_2SDBA (4,4′-sulfonyldibenzoic acid) and was evaluated for the sensing capability for vapors of selected VOCs and nitroaromatic compounds. It was demonstrated that the trimetallic analogue **UCY-15**($Y_{0.875}Eu_{0.05}Tb_{0.075}$) is sensitive towards a variety of analytes at very low concentrations.[23] A common feature in the synthesis of MOFs based on polynuclear SBUs with RE^{3+} ions is the utilization of modulators such as 2-fluorobenzoic acid (HFBA), or alternatively, 2,6-difluorobenzoic acid (HF_2BA). These acids apart from preventing the formation of one-dimensional chain SBUs with RE^{3+} ions also significantly increase the quality of the single crystals obtained during the synthesis. However, recent publications concerning RE-MOFs synthesized utilizing HFBA or HF_2BA indicated the existence of μ_3-F^- bridging ions in the structural core of the MOFs.[23,60–62] Thus, HFBA and HF_2BA were proven to act not only as modulators but also as reactants providing F^- anions to the reaction mixture.[63] A series of reactions have been explored involving various angular dicarboxylic ligands, containing two benzoic acid moieties linked through various central groups. Most of these ligands were commercially available and have been widely employed in MOF chemistry; however, ligands that were synthesized by using other precursor compounds were also employed in these efforts. One of them is H_2BCPM, the reduced analogue of 4,4′-carbonyldibenzoic acid, H_2BPHD (the ketone group has been reduced to an alcohol one) which has not been widely used in MOF chemistry. In fact, to the best of our knowledge there are no RE-MOFs reported in the literature with this ligand and very few compounds with any metal ion.[64,65] We explored reactions of H_2BCPM with RE^{3+} salts in the presence of HFBA targeting analogues of **UCY-13**, **UCY-14** and **UCY-15**. These synthetic efforts involved the use of various RE^{3+} salt/H_2BCPM molar ratios and reaction conditions (solvent system, addition of concentrated acids and the reaction temperature). Thus, the reaction of $RE(NO_3)_3{\cdot}xH_2O$ (x = 5 or 6) with H_2BCPM in a molar ratio of 1 : 2.5 in DMF/H_2O in the presence of ~7 equivalents of HFBA at 115 °C for five days afforded colourless rhombic crystals of compounds **UCY-17**(RE); (RE: Y, Gd, Tb, Dy, Ho, and Er). The experimental pXRD patterns of **UCY-17**(RE) analogues along with the simulated one of **UCY-17**(Tb) and IR spectra are shown in Fig. S1 and S2 in the ESI.†

The structure of compound **UCY-17**(RE); (RE: Y, Gd, Tb, Dy, Ho, and Er) crystallizing in the monoclinic space group $C2/m$ contains two crystallographically independent RE^{3+} ions. Since the **UCY-17**(RE) compounds are isostructural, crystallize in the same space group with similar unit cell dimensions and their main difference is the RE^{3+} ion that is present in each structure, only the structure of **UCY-17**(Tb) will be discussed in detail. Representations of the structure of **UCY-17**(Tb) along the axes a, b and c are shown in Fig. 1. Tb1 and Tb2 ions are coordinated to eight oxygen atoms adopting a square antiprismatic geometry.[66] In particular, the coordination environment of Tb1 consists of four μ_3-OH^- monoatomic bridges, two carboxylate oxygen atoms of two bridging $BCPM^{2-}$ ligands, one oxygen atom of a bridging NO_3^- ion and a terminal water molecule. In addition, the coordination sphere of Tb2 contains four μ_3-OH^- monoatomic bridges and four carboxylate oxygen atoms from four bridging $BCPM^{2-}$ ligands. The existence of μ_3-F^- anions in this compound was confirmed by recording ^{19}F-NMR spectra of a digested sample of **UCY-17**(Tb) which

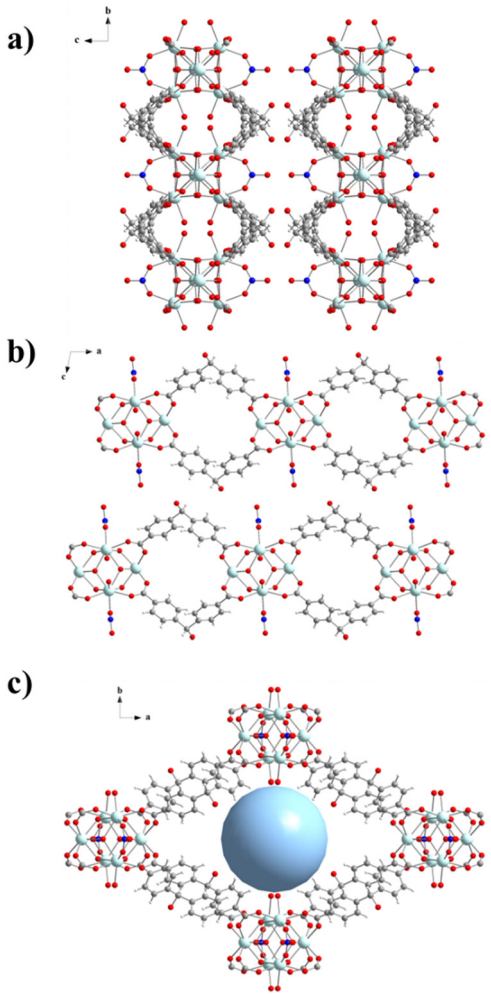

Fig. 1 Representations of the structure of **UCY-17**(Tb) along the (a) *a*, (b) *b* and (c) *c* axes. The cyan sphere (shown in (c)) denotes the pores formed between the parallel layers along the *c*-axis. Colour code: Tb, light blue; O, red; N, blue; C, grey; and H, white.

suggests the existence of around two F^- ions per $(Tb^{3+})_6$ SBU (Fig. S3–S5, ESI†).[21,60,62] Thus, the SBU of **UCY-17**(Tb) is a hexanuclear cluster containing a $[Tb_6(\mu_3\text{-}OH^-/F^-)_8]^{10+}$ structural core in which the Tb^{3+} ions are located in the vertices of an octahedron and the μ_3-OH^-/F^- bridges lie above its faces. The peripheral ligation of the hexanuclear cluster is completed by eight carboxylate groups of $BCPM^{2-}$ ligands adopting the common *syn*, *syn*-η^1:η^1:μ coordination mode, two bridging NO_3^- anions connecting two Tb1 ions and four terminal H_2O molecules also ligated to Tb1 centers. The hexanuclear SBUs are linked through eight $BCPM^{2-}$ ligands, with each pair of them connecting two adjacent $(Tb^{3+})_6$ SBUs. As a result, the eight $BCPM^{2-}$ ligands connect the hexanuclear SBU with four neighbouring SBUs giving rise to a neutral 2-dimensional nanosheet with a thickness of ~13 Å. The 2D layers display two types of rhombic cavities with dimensions ~11.5 × 13 $Å^2$ and ~10 × 24 $Å^2$ along *b*- and *c*-axes, respectively (Fig. 1b and c). The 2-D layers are fairly well separated with the shortest interlayer distance appearing between the alcohol O atom and a C atom of a benzene ring of the $BCPM^{2-}$ ligand of adjacent layers being ~3.90 Å. As a result, there are no significant interlayer interactions between neighbouring layers. The solvent accessible volume of the framework corresponds to ~65% of the unit cell volume. Although several examples of RE^{3+} MOFs based on the hexanuclear SBU have been reported, the vast majority are 3D compounds.[18,59,67–72] To the best of our knowledge, compound **UCY-17**(RE) is only the third example of a 2D MOF based on the $(RE^{3+})_6$-SBU.[23,40] It is also noted that its structure displays analogies to that of compound **UCY-15**[23] with both of them comprising a rare 8-connected 2D network based on the $(RE^{3+})_6$ SBU. However, they differ in the organic bridging ligand they contain ($BCPM^{2-}$ in **UCY-17**(RE) and $SDBA^{2-}$ in **UCY-15**), the number of terminal H_2O molecules (4 in **UCY-17**(RE) and 6 in **UCY-15**) and the coordination number/coordination geometry of the lanthanide ions (all metal ions are 8-coordinated in **UCY-17**(RE) whereas there are 8- and 9-coordinated lanthanide ions in **UCY-15**) and the presence (in **UCY-15**) or absence (in **UCY-17**(RE)) of interlayer hydrogen bonding interactions.

The stability of compound **UCY-17**(Tb) treated in various organic solvents was studied with pXRD which indicated that the compound retains its crystallinity and structural integrity in most organic solvents (Fig. S6, ESI†). In addition, the thermal stability of **UCY-17**(RE) analogues was studied with thermogravimetric analysis (Fig. S7, ESI†). The thermal decomposition of compounds **UCY-17**(RE) proceeds *via* a two-step process (Fig S7, ESI†). The first step (until ~450–460 °C) is attributed to the removal of the terminal H_2O and lattice DMF molecules. The second mass loss which is completed at ~620–640 °C is attributed to the decomposition of the ligand $BCPM^{2-}$. The residual mass at 900 °C corresponds to the rare earth oxide of the corresponding RE^{III} ion (Table S4, ESI†).

Single-crystal-to-single-crystal transformations

UCY-17(RE) analogues crystallize in high yields and form excellent quality single-crystals, with a high solvent accessible volume and relatively large 1-D channels. In addition, they contain labile bridging NO_3^- ions located, in proximity, in adjacent 2D-nanosheets. In fact, the distance between the bound O atoms of two adjacent NO_3^- anions (~6.85 Å) (Fig. 1a.) is comparable to the separation between carboxylic oxygen atoms of H_2BDC (which is ~6.9 Å) and other derivatives containing functional groups in the phenyl ring. For these reasons this compound was considered for the investigation of SCSC linker installation reactions.

Thus, heterogeneous reactions of single crystals of **UCY-17**(Tb) with solutions of a dicarboxylic ligand (25 mM in DMF) were performed at an elevated temperature (~80 °C). The reactions resulted in single crystals which were macroscopically very similar in size and shape to those of the pristine compound **UCY-17**(Tb); however, they contained cracks resulting from treatment under intense conditions and/or the insertion of bulky organic molecules (Fig. S8, ESI†). X-ray structural determination of the exchanged analogues revealed that compounds **UCY-17**(Tb)/L are similar to the pristine structure

regarding the connectivity of the initial 2-D framework but the connectivity of the SBUs and the dimensionality of the framework are increased in the exchanged analogues from 8-c to 10-c and from 2-D to 3-D, respectively. Specifically, all SCSC products crystallize in the same space group as the pristine compound (*C*2/*m*) and the $[Tb_6(\mu_3\text{-}OH)_8]^{10+}$structural core of the hexanuclear SBU remains intact. However, the introduction of a second dicarboxylate ligand in the structure of **UCY-17**(Tb) results in the increase of the connectivity of the SBU from 8-c to 10-c since each SBU is not only bridged by eight $BCPM^{2-}$ ligands to four neighbouring SBUs along the *ab*-plane but also to two L^{2-} ligands which link the 2-D frameworks along the *c*-axis thus forming 3-D neutral frameworks (Fig. 2 and 3). Additionally, the introduction of the second dicarboxylic linker connecting the secondary building units of two different 2D sheets results in different spacing between the adjacent 2-D nanosheets suggesting the breathing of the structure of the pristine **UCY-17**(Tb) MOF which facilitates the insertion of the dicarboxylic linkers. This is supported by the comparison of the shorter Tb···Tb separations between adjacent 2-D sheets in the pristine **UCY-17**(Tb) (10.854 Å) and the exchanged analogues **UCY-17**(Tb)/BDC (11.017 Å), **UCY-17**(Tb)/ABDC (11.140 Å), **UCY-17**(Tb)/FBDC (11.115 Å) and **UCY-17**(Tb)/NDC (11.265 Å) which reveals that these are larger in the latter. In fact, the larger Tb···Tb separation appears as expected in **UCY-17**(Tb)/NDC which contains the bulkier dicarboxylic ligand.

Another interesting structural modification that took place in compounds **UCY-17**(Tb)/NDC involved a different coordination mode of the carboxylate groups than those appearing in the other exchanged analogues and the pristine compound (for the NO_3^- ligand). In particular, each NO_3^- ligand in the pristine compound bridges two Tb^{3+} ions adopting a *syn–syn* mode as happens with the two carboxylate groups of the installed dicarboxylic ligands in compounds **UCY-17**(Tb)/L; (L = BDC^{2-}, $ABDC^{2-}$, and $FBDC^{2-}$) which bridge four Tb^{3+} ions in a $\eta^1{:}\eta^1{:}\eta^1{:}\eta^1{:}\mu_4$ coordination mode. However, in the **UCY-17**(Tb)/NDC analogue the NDC^{2-} linker bridges three metal ions adopting a $\eta^1{:}\eta^1{:}\eta^1{:}\eta^1{:}\mu_3$ mode with one carboxylate group chelated on a Tb^{3+} ion and a second one bridging in a *syn–syn* mode (Fig. 3). In fact, this is the first time that such variability in the bridging modes of the dicarboxylic ligands inserted through SCSC linker installation reactions in the family of MOFs based on hexanuclear SBUs is observed. The solvent accessible volume for the exchanged analogues **UCY-17**(Tb)/L as calculated using PLATON software ranges between 64% and 65% which remains unchanged compared to that of the pristine compound **UCY-17**(Tb).[57]

Apart from the existence of various bridging modes of the inserted bridging dicarboxylic ligands, there are a series of other interesting structural features in the obtained exchanged analogues. Although there are examples of 2-D MOFs based on 3d metal ions transformed into 3-D ones,[73] the conversion of a

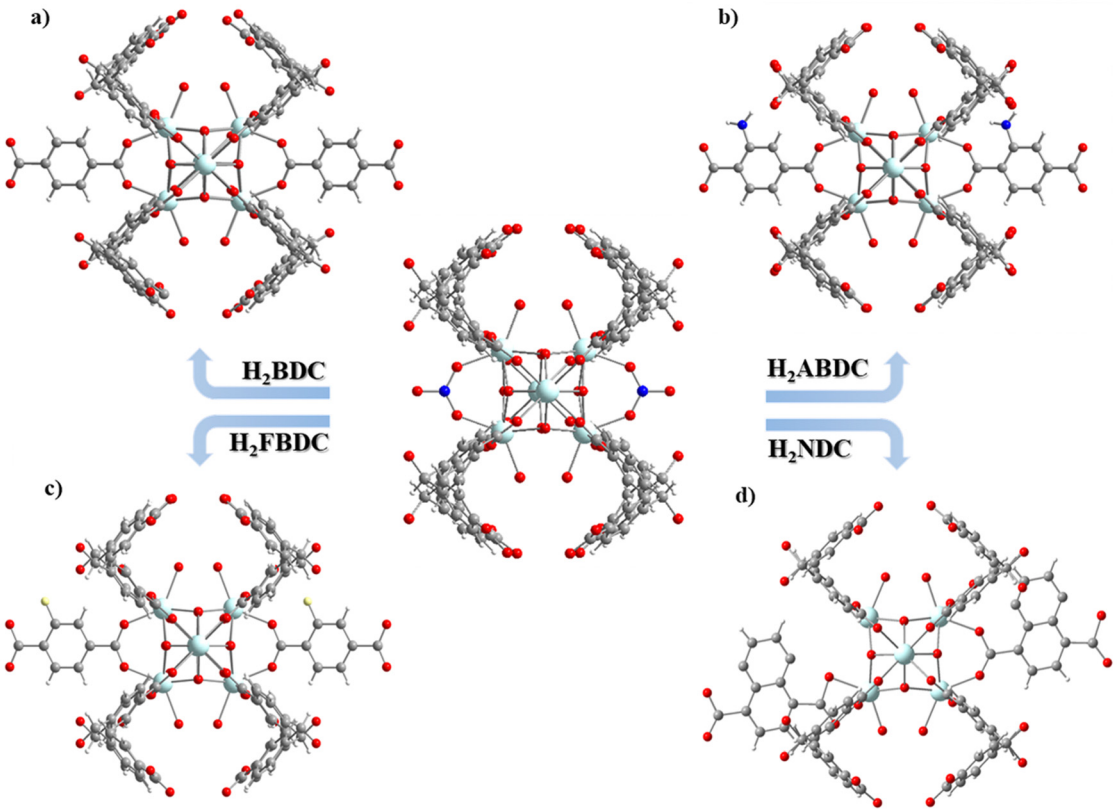

Fig. 2 Representations of the SBUs of **UCY-17**(Tb) (in the center) and of: (a) **UCY-17**(Tb)/BDC, (b) **UCY-17**(Tb)/ABDC, (c) **UCY-17**(Tb)/FBDC and (d) **UCY-17**(Tb)/NDC. Colour code: Tb, light blue; F, light yellow; O, red; N, blue; C, grey; and H, white.

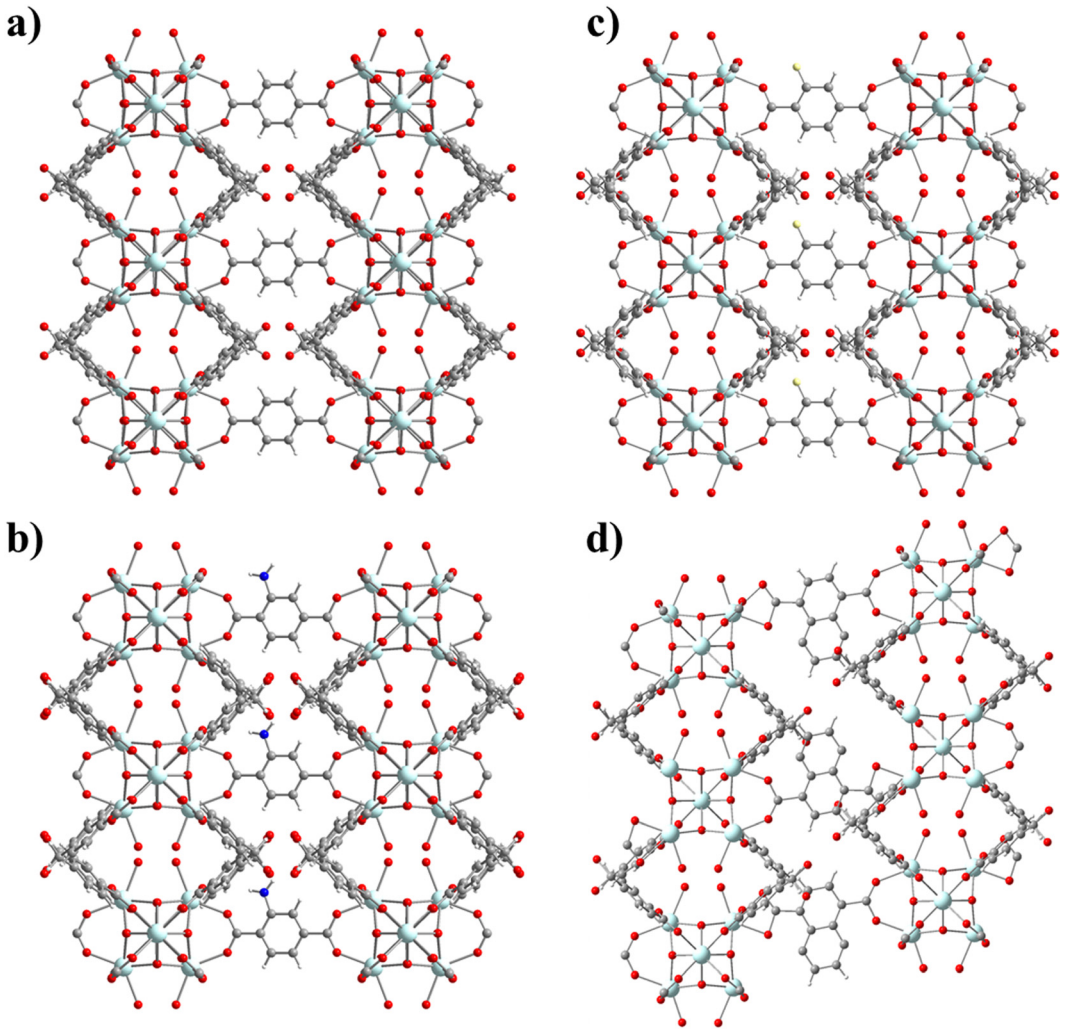

Fig. 3 Representations of the structures of (a) **UCY-17**(Tb)/BDC (b) **UCY-17**(Tb)/ABDC, and (c) **UCY-17**(Tb)/FBDC along the *a* axis and (d) **UCY-17**(Tb)/NDC along the *b* axis. Colour code: Tb, light blue; F, light yellow; O, red; N, blue; C, grey; and H, white.

2-D, 8-c RE^{3+} MOF to a 3-D one through a SCSC linker installation reaction takes place for the first time in the literature. There is only one other example of a 2-D RE^{3+} MOF that is modified to a 3-D one, but this involves a 6-c pristine MOF that is modified to a 12-c 3-D one. In fact, the 3-D MOFs that are produced from the linker installation reactions are uncommon examples of 10-connected MOFs; a Cambridge database search revealed that there are a few 10-c Zr^{4+} MOFs based on hexanuclear SBUs[35] and one family of RE^{3+} ones.[74] Thus, in this case, the linker installation process provided access to very uncommon examples of 10-c RE^{3+} MOFs based on hexanuclear SBUs.

PXRD studies and IR spectra of the exchanged analogues confirmed that the crystallinity and structural integrity of compounds **UCY-17**(RE)/L are retained upon SCSC reactions (Fig. S9–S12, ESI†). Thermal analysis revealed that the TG plots for the exchanged analogues **UCY-17**(Tb)/L have a similar profile as the pristine MOF **UCY-17**(Tb) and their decomposition is also completed in two steps (Fig. S13 and Table S5, ESI†). In addition, the stability of the pristine MOF **UCY-17**($Eu_{0.05}Tb_{0.95}$) and the exchanged analogues **UCY-17**($Eu_{0.05}Tb_{0.95}$)/L heated at ~90 °C (following a process that is described in the experimental part) was investigated and it was confirmed that their structure remains intact up to this temperature (Fig. S14 and S15, ESI†).

Photophysical properties

Room-temperature photoluminescence properties of **UCY-17**(RE) (RE: Gd, Tb, and $Eu_{0.05}Tb_{0.95}$), the exchanged analogues **UCY-17**(RE)/L (RE: Tb, $Eu_{0.05}Tb_{0.95}$) and the ligands were investigated in the solid state as crystalline powders. Upon excitation at ~350 nm, a broad emission band at 400 nm is observed in the PL spectra of H_2BCPM which is attributed to the $\pi^* \rightarrow \pi$ transition of the ligand[65] (Fig. S16 and S17, ESI†). Further studies included the measurement of the PL spectra of **UCY-17**(Gd) where the excitation and emission bands are slightly shifted compared to the corresponding signals of the H_2BCPM ligand. Specifically, a broad emission band at 400 nm is observed upon excitation at ~350 nm which is also attributed to the $\pi^* \rightarrow \pi$ transition of the anion of $BCPM^{2-}$ (Fig. S16,

ESI†). **UCY-17**(Tb) displays the characteristic PL signals of Tb^{3+} ions upon excitation at 345 nm. It should be noted that in this region only $BCPM^{2-}$ absorbs light which sensitizes Tb^{3+} ions through energy transfer. Thus, **UCY-17**(Tb) displays strong and sharp emission bands at 487, 545, 582 and 620 nm which are attributed to the $^5D_4 \rightarrow {}^7F_J$ (J = 6, 5, 4 and 3, respectively) transitions (Fig. S17, ESI†). Room-temperature emission spectra of **UCY-17**(Tb)/L analogues, upon UV excitation at ~350 nm, revealed that these exchanged analogues display different behaviour, both in comparison with each other and also to the pristine **UCY-17**(Tb) MOF. The room-temperature emission spectra of all samples display emission bands at 487, 545, 582 and 620 nm which are attributed to the $^5D_4 \rightarrow {}^7F_J$ (J = 6, 5, 4 and 3, respectively) transitions of Tb^{3+} ions. However, the relative intensity of the ligand-based emission bands at ~400 nm compared to the intensity of the Tb^{3+} transitions is different in each case due to the introduction of the second linker in the framework of **UCY-17**(Tb) which perturbs the energy transfer processes occurring during relaxation of excited **UCY-17**(Tb)/L (*vide infra*) (Fig. S16 and S17, ESI†).

Upon UV excitation, the room-temperature emission spectra of the pristine MOF **UCY-17**($Eu_{0.05}Tb_{0.95}$) and the exchanged analogues **UCY-17**($Eu_{0.05}Tb_{0.95}$)/L display the main signals at 490 and 545 nm of Tb^{3+}, and at 587, 611, and 695 nm for Eu^{3+}, attributed to the $^5D_4 \rightarrow {}^7F_{6\text{-}3}$ and the $^5D_0 \rightarrow {}^7F_{0\text{-}4}$ transitions of Tb^{3+} and Eu^{3+}, respectively (Fig. 4a). The relative intensity of the main Tb^{3+} ion emission (at 545 nm) changes according to the nature of the inserted dicarboxylate ligand. Therefore, under UV excitation, the emission colour of all samples varies from green to red, as suggested by the CIE chromatic coordinates (x,y) (Fig. 4b and Table S6, ESI†). Room-temperature excitation spectra monitored on all compounds evidence the presence of $^7F_6 \rightarrow {}^5D_4$ Tb^{3+} transition (at ~490 nm) within the $^5D_0 \rightarrow {}^7F_2$ Eu^{3+} transition (Fig. S18 and S19, ESI†) which confirms the occurrence of Tb^{3+}-to-Eu^{3+} energy transfer in mixed Ln^{3+} compounds.

Steady state and time-resolved spectroscopy techniques were used to estimate the energy of the triplet level of the pristine **UCY-17**(Gd) MOF (Fig. S20, ESI†). Phosphorescence spectra of the pristine **UCY-17**(Gd) MOF and its exchanged analogues were monitored at 77 K to estimate the energy of the triplet (T_1) level. Consequently, the T_1 level of the $BPCM^{2-}$ ligand was estimated to be 24 400 cm^{-1}, which is in a suitable energy range to sensitize both Eu^{3+} and Tb^{3+} ions according to Latva's empirical rule.[75] For compounds **UCY-17**(Gd)/L (Fig. S21, ESI†), the phosphorescence spectrum at 77 K corresponds to the combination of emission from the T_1 level of both bridging ligands, namely $BPCM^{2-}$ and the inserted dicarboxylate one. Thus, for the exchanged analogue **UCY-17**(Gd)/BDC, the emission spectrum at 77 K (Fig. S21a, ESI†) and the resulting T_1 value of 24 350 cm^{-1} are similar to these of the pristine **UCY-17**(Gd) MOF indicating that the inserted BDC^{2-} ligand does not affect them significantly. That is why the sensitization of Eu^{3+} and Tb^{3+} ions in the **UCY-17**(Gd)/BDC compound is similar to that of the pristine material, as evidenced by their similar CIE coordinates (Fig. 4b). The same behavior was observed for the

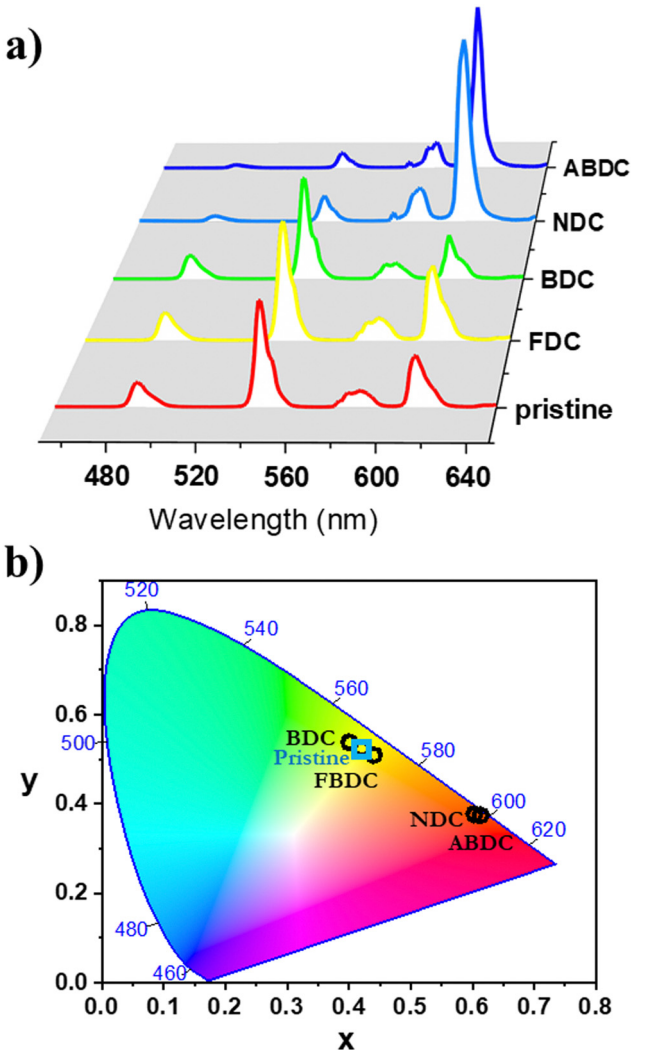

Fig. 4 (a) Room-temperature emission spectra and (b) CIE chromaticity diagram of the pristine MOF **UCY-17**($Eu_{0.05}Tb_{0.95}$) and the exchanged analogues **UCY-17**($Eu_{0.05}Tb_{0.95}$)/L calculated from the emission spectra (λ_{exc} = 309 nm).

exchanged analogue **UCY-17**(Gd)/FBDC (T_1 = 24 420). On the other hand, for exchanged analogues **UCY-17**(Gd)/ABDC and **UCY-17**(Gd)/NDC, the emission spectra at 77 K (Fig. S21b and d, ESI†) and the resulting T_1 values of 21 700 and 19 600 cm^{-1}, respectively, deviate significantly from these of the pristine **UCY-17**(Gd) (see above and Fig. S20, ESI†). This suggests the dominating role of the inserted dicarboxylate ligands in the phosphorescence spectra of **UCY-17**(Gd)/ABDC and **UCY-17**(Gd)/NDC. The result of the significant decrease of the T_1 values of the two exchanged analogues compared to the pristine **UCY-17**(Gd) MOF is the less efficient sensitization of Tb^{3+}, with a $^5D_4$ level of 20 500 cm^{-1}.[76] This is confirmed by the emission spectra of **UCY-17**($Eu_{0.05}Tb_{0.95}$)/ABDC and **UCY-17**($Eu_{0.05}Tb_{0.95}$)/NDC where the Eu^{3+} red emission is predominant for both compounds (Fig. 4a) and their very different CIE coordinates than those of the pristine **UCY-17**($Eu_{0.05}Tb_{0.95}$) MOF and the exchanged analogues **UCY-17**($Eu_{0.05}Tb_{0.95}$)/BDC and **UCY-17**($Eu_{0.05}Tb_{0.95}$)/FBDC (Fig. 4b).

Thermometric properties

The application of the mixed Eu–Tb **UCY-17**($Eu_{0.05}Tb_{0.95}$) MOF and its exchanged derivatives as temperature sensors was tested using their emission spectra. It is known that the thermometric properties of MOFs are affected by the organic ligands in their structure, since their triplet energy level influences the relative thermal sensitivity.[77] For this reason it was anticipated that the insertion of selected bridging dicarboxylic ligands in the structure of **UCY-17**($Eu_{0.05}Tb_{0.95}$) could lead to significant modifications of its thermometric performance.

The integrated areas of the $^5D_4 \rightarrow {}^7F_5$ (I_{Tb}) and $^5D_0 \rightarrow {}^7F_2$ (I_{Eu}) emissions were used to define the thermometric parameter as $\Delta = I_{Tb}/I_{Eu}$. The I_{Tb} and I_{Eu} areas were integrated using the emission spectra in the 535–565 nm and 602–637 nm intervals, respectively. These studies revealed that the pristine **UCY-17**($Eu_{0.05}Tb_{0.95}$) MOF does not present any thermal evolution of the integrated emission intensities between 270 and 360K or even between 80 and 300 K but only some small fluctuations (that do not exceed ~5% of the maximum integrated emission intensity) (Fig. S22 and S27, ESI†). Consequently, this material is not a good candidate for a luminescent thermometer. On the other hand, the exchanged derivatives **UCY-17**($Eu_{0.05}Tb_{0.95}$)/L exhibit notable temperature dependence of their integrated intensity (around 40%) (Fig. 5 and Fig. S23–S26, ESI†). Interestingly, the temperature dependence plot of I_{Tb} and I_{Eu} for each exchanged analogue has a different profile, depending on the inserted bridging dicarboxylate ligand through linker installation reactions. Thus, for **UCY-17**($Eu_{0.05}Tb_{0.95}$)/BDC the integrated emissions increase from 300 to 350 K (40% for I_{Eu} and 15% for I_{Tb}) whereas for **UCY-17**($Eu_{0.05}Tb_{0.95}$)/ABDC both Eu^{3+} and Tb^{3+} emissions decrease from 313 to 353 K with the same tendency. In addition, for **UCY-17**($Eu_{0.05}Tb_{0.95}$)/FBDC and **UCY-17**($Eu_{0.05}Tb_{0.95}$)/NDC exchanged analogues, the intensity of Tb^{3+} continuously decreases from 273 K while I_{Eu} concomitantly increases with an increase in temperature.

Although the phenomenological Mott–Seitz expression is typically used to model the thermal evolution of the thermometric parameter Δ,[43,48,76,78] in this study it did not allow to correctly fit the calibration curves $\Delta = f(T)$. Consequently, a polynomial function was arbitrarily chosen to simulate the curves $\Delta = f(T)$; the obtained fits are shown in Fig. S28 (ESI†) and the fitting parameters are reported in Table S7 (ESI†). The corresponding relative thermal sensitivity, defined as $S_r = |\partial\Delta/\partial T|/\Delta$ and used as a figure of merit to compare the performance of distinct systems,[76,79,80] is plotted in Fig. 6. The **UCY-17**($Eu_{0.05}Tb_{0.95}$)/L exchanged analogues exhibit a thermal sensitivity above room temperature, with the maximum S_m values appearing between ~300 and 355 K (Fig. 6); studies at higher temperatures were not conducted due to the decomposition of compounds above 373 K (Fig. S13 and S14, ESI†). Among the exchanged analogues, the **UCY-17**($Eu_{0.05}Tb_{0.95}$)/ABDC compound is the most sensitive material with a maximum relative thermal sensitivity (S_m) of 1.1% K^{-1} at 353 K. The S_m values of remaining exchanged analogues were found to be S_m = 1% K^{-1} at 328 K for **UCY-17**($Eu_{0.05}Tb_{0.95}$)/FBDC and S_m = 0.56% K^{-1} at 304 K for **UCY-17**($Eu_{0.05}Tb_{0.95}$)/NDC, and S_m = 0.53% K^{-1} at 323 K for **UCY-17**($Eu_{0.05}Tb_{0.95}$)/BDC.

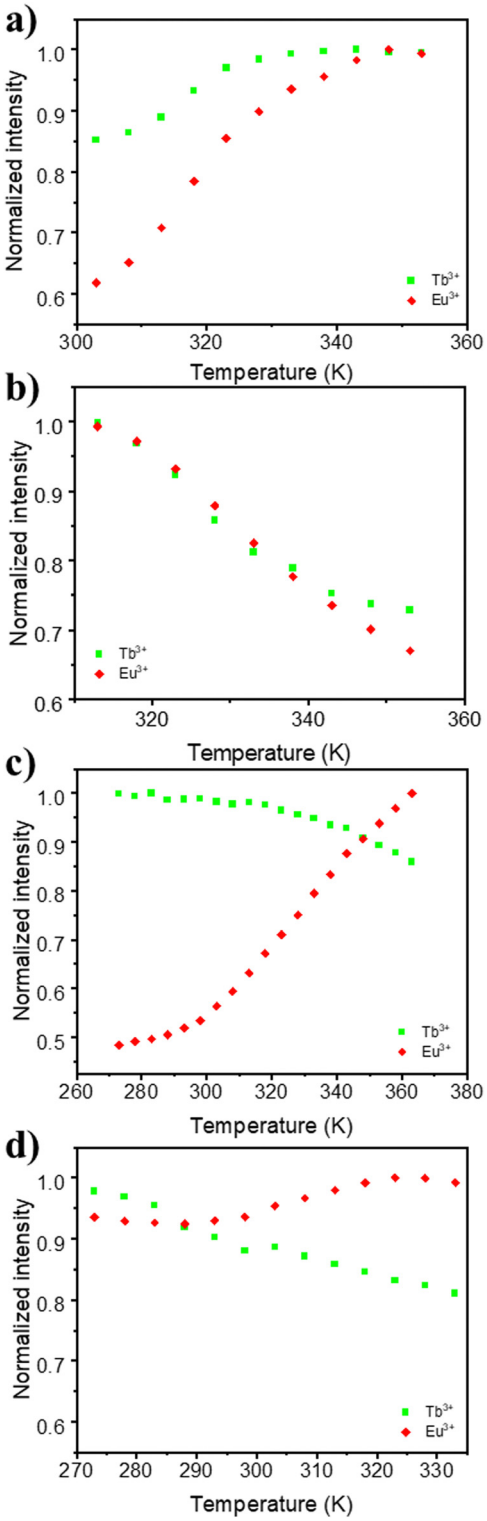

Fig. 5 Thermal evolution of the integrated emission intensity of the exchanged analogues: (a) **UCY-17**($Eu_{0.05}Tb_{0.95}$)/BDC, (b) **UCY-17**($Eu_{0.05}Tb_{0.95}$)/ABDC, (c) **UCY-17**($Eu_{0.05}Tb_{0.95}$)/FBDC, and (d) **UCY-17**($Eu_{0.05}Tb_{0.95}$)/NDC.

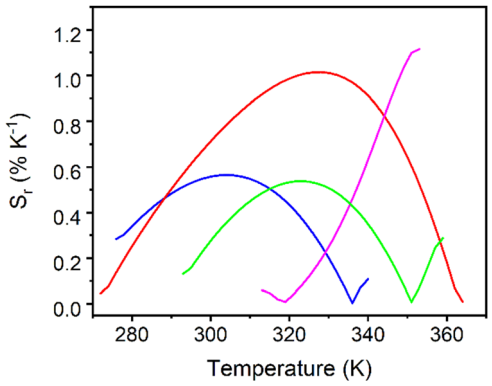

Fig. 6 Relative thermal sensitivity of the exchanged analogues **UCY-17**($Eu_{0.05}Tb_{0.95}$)/BDC (green solid line), **UCY-17**($Eu_{0.05}Tb_{0.95}$)/ABDC (pink solid line), **UCY-17**($Eu_{0.05}Tb_{0.95}$)/FBDC (red solid line), and **UCY-17**($Eu_{0.05}Tb_{0.95}$)/NDC (blue solid line).

Conclusions

Rare examples of 2-dimensional RE^{3+} MOFs based on an eight-connected hexanuclear $(RE^{3+})_6$ SBU are reported with the formula $[RE_6(\mu_3\text{-}OH^-/F^-)_8(BCPM)_4(NO_3)_2(H_2O)_4]_n$ (**UCY-17**(RE) RE: Y, Gd, Tb, Dy, Ho, Er). The ideal distance (similar to the size of various aromatic dicarboxylic ligands) between adjacent 2-D layers of **UCY-17**(RE) allowed the targeted replacement, through SCSC linker installation reactions, of the NO_3^- anions bridging two RE^{3+} ions of the hexanuclear SBU by a series of dicarboxylate linkers. This replacement gave rise to the increase of the dimensionality of these MOFs and the formation of uncommon 10-connected 3-D RE^{3+} MOFs with the formula $[RE_6(\mu_3\text{-}OH^-/F^-)_8(BCPM)_4(L)(H_2O)_4]_n$ (L = BDC^{2-}, $ABDC^{2-}$, $FBDC^{2-}$ and NDC^{2-}). In fact, this is the second example of a 2-D MOF based on a hexanuclear SBU that is converted through an SCSC linker installation reaction to a 3-D one; the other example involved a 6-connected 2-D RE^{3+} MOF that was converted to a 12-connected 3-D MOF. The photophysical and thermometric properties of the bimetallic Eu–Tb pristine MOF **UCY-17**($Eu_{0.05}Tb_{0.95}$) and the exchanged analogues **UCY-17**($Eu_{0.05}Tb_{0.95}$)/L were studied to investigate how these are affected by the insertion of the dicarboxylic linkers into the structures of these MOFs. In fact, these compounds were ideal for this purpose since despite the insertion of the dicarboxylic ligands and the increase of the dimensionality of MOFs the main structural features including the coordination number and geometry of metal ions remained essentially unaffected upon SCSC linker installation reactions. Interestingly, a variety of different behaviours was observed in compounds **UCY-17**($Eu_{0.05}Tb_{0.95}$) and **UCY-17**/L concerning the profile of the room temperature emission spectra, the energy of T_1 states and the Tb^{3+} sensitization efficiency of the pristine and exchanged analogues depending on the type of the inserted bridging dicarboxylates. A similar wealth of different behaviours were also observed from the investigation of the thermometric properties of the pristine MOF **UCY-17**($Eu_{0.05}Tb_{0.95}$) and the exchanged analogues **UCY-17**($Eu_{0.05}Tb_{0.95}$)/L. In particular, the pristine MOF did not display thermal evolution of the integrated emission intensities in the temperature range that was investigated (80–360 K). On the other hand, the exchanged analogues displayed notable temperature dependence of the emission intensities and the temperature dependence plot of I_{Tb} and I_{Eu} for each exchanged analogue exhibited a different profile, depending on the inserted bridging dicarboxylate ligand. As a result, their maximum thermal sensitivities appeared at different temperatures ranging from ~300 to 355 K. This significant variation observed in the photophysical and thermometric properties of the reported compounds took place because of the presence of a series of different dicarboxylic ligands in these compounds which affected significantly the photophysical and thermometric properties of the MOFs. This work sheds light on how the photophysical and thermometric properties of MOFs based on the hexanuclear RE^{3+} SBU are affected by the insertion of a variety of simple bridging dicarboxylic ligands and highlights the role of the SCSC linker installation method in tuning the thermometric properties of lanthanide MOFs. Finally, it suggests a rational method for the enhancement of the thermometric properties of MOFs that could allow the design of new performant luminescent thermometers based on RE_6-MOFs.

Author contributions

Laoura Komodiki: investigation, methodology, and writing – original draft. Nikos Panagiotou: investigation, methodology, and writing – original draft. Hélène Serier-Brault: investigation, methodology, project supervision, and writing – original draft, reviewing and editing. Anastasios J. Tasiopoulos: project supervision and manuscript writing – reviewing and editing.

Conflicts of interest

There are no conflicts to declare.

Acknowledgements

This work was funded under the M-ERA.NET Call 2019 and the Republic of Cyprus through the Research and Innovation Foundation (contract no. P2P/M-ERA.NET/0319/0005; Acronym: SALMOS).

References

1 H. Furukawa, K. E. Cordova, M. O'Keeffe and O. M. Yaghi, The chemistry and applications of metal-organic frameworks, *Science*, 2013, **341**, 1230444, DOI: 10.1126/science.1230444.
2 D. Alezi, Y. Belmabkhout, M. Suyetin, P. M. Bhatt, L. J. Weseliński, V. Solovyeva, K. Adil, I. Spanopoulos, P. N. Trikalitis, A. H. Emwas and M. Eddaoudi, MOF Crystal Chemistry Paving the Way to Gas Storage Needs: Aluminum-

Based soc -MOF for CH_4, O_2, and CO_2 Storage, *J. Am. Chem. Soc.*, 2015, **137**, 13308.

3 O. T. Qazvini, V. J. Scott, L. Bondorf, M. Ducamp, M. Hirscher, F. X. Coudert and S. G. Telfer, Flexibility of a Metal-Organic Framework Enhances Gas Separation and Enables Quantum Sieving, *Chem. Mater.*, 2021, **33**, 8886.

4 S. Krause, N. Hosono and S. Kitagawa, Chemistry of Soft Porous Crystals: Structural Dynamics and Gas Adsorption Properties, *Angew. Chem., Int. Ed.*, 2020, **59**, 15325.

5 T. Simon-Yarza, A. Mielcarek, P. Couvreur and C. Serre, Nanoparticles of Metal-Organic Frameworks: On the Road to In Vivo Efficacy in Biomedicine, *Adv. Mater.*, 2018, **30**, 1.

6 E. A. Dolgopolova, A. M. Rice, C. R. Martin and N. B. Shustova, Photochemistry and photophysics of MOFs: steps towards MOF-based sensing enhancements, *Chem. Soc. Rev.*, 2018, **47**, 4710.

7 J. F. Olorunyomi, S. T. Geh, R. A. Caruso and C. M. Doherty, Metal-organic frameworks for chemical sensing devices, *Mater. Horiz.*, 2021, **8**, 2387.

8 W. M. Chen, X. L. Meng, G. L. Zhuang, Z. Wang, M. Kurmoo, Q. Q. Zhao, X. P. Wang, B. Shan, C. H. Tung and D. Sun, A superior fluorescent sensor for Al^{3+} and UO_2^{2+} based on a Co(II) metal-organic framework with exposed pyrimidyl Lewis base sites, *J. Mater. Chem. A*, 2017, **5**, 13079.

9 T. Wang, Y. Jia, Q. Chen, R. Feng, S. Tian, T. L. Hu and X. H. Bu, A new luminescent metal-organic framework for selective sensing of nitroaromatic explosives, *Sci. China: Chem.*, 2016, **59**, 959.

10 L. Gan, M. T. Nord, J. M. Lessard, N. Q. Tufts, A. Chidambaram, M. E. Light, H. Huang, E. Solano, J. Fraile, F. Suárez-García, C. Viñas, F. Teixidor, K. C. Stylianou and J. G. Planas, Biomimetic Photodegradation of Glyphosate in Carborane-Functionalized Nanoconfined Spaces, *J. Am. Chem. Soc.*, 2023, **145**, 13730.

11 M. Zhao, S. Huang, Q. Fu, W. Li, R. Guo, Q. Yao, F. Wang, P. Cui, C. H. Tung and D. Sun, Ambient Chemical Fixation of CO_2 Using a Robust Ag_{27} Cluster-Based Two-Dimensional Metal–Organic Framework, *Angew. Chem., Int. Ed.*, 2020, **59**, 20031.

12 M. O'keeffe, Design of MOFs and intellectual content in reticular chemistry: A personal view, *Chem. Soc. Rev.*, 2009, **38**, 1215.

13 D. J. O'Hearn, A. Bajpai and M. J. Zaworotko, The ''Chemistree'' of Porous Coordination Networks: Taxonomic Classification of Porous Solids to Guide Crystal Engineering Studies, *Small*, 2021, **17**, 1.

14 Y. Liu, V. C. Kravtsov, R. Larsen and M. Eddaoudi, Molecular building blocks approach to the assembly of zeolite-like metal-organic frameworks (ZMOFs) with extra-large cavities, *Chem. Commun.*, 2006, 1488.

15 M. Eddaoudi, D. B. Moler, H. Li, B. Chen, T. M. Reineke, M. O'Keeffe and O. M. Yaghi, Modular chemistry: Secondary building units as a basis for the design of highly porous and robust metal-organic carboxylate frameworks, *Acc. Chem. Res.*, 2001, **34**, 319.

16 J. H. Cavka, S. Jakobsen, U. Olsbye, N. Guillou, C. Lamberti, S. Bordiga and K. P. Lillerud, A new zirconium inorganic building brick forming metal organic frameworks with exceptional stability, *J. Am. Chem. Soc.*, 2008, **130**, 13850.

17 S. Yuan, L. Feng, K. Wang, J. Pang, M. Bosch, C. Lollar, Y. Sun, J. Qin, X. Yang, P. Zhang, Q. Wang, L. Zou, Y. Zhang, L. Zhang, Y. Fang, J. Li and H. C. Zhou, Stable Metal–Organic Frameworks: Design, Synthesis, and Applications, *Adv. Mater.*, 2018, **30**, 1.

18 D. X. Xue, A. J. Cairns, Y. Belmabkhout, L. Wojtas, Y. Liu, M. H. Alkordi and M. Eddaoudi, Tunable rare-earth fcu-MOFs: A platform for systematic enhancement of CO_2 adsorption energetics and uptake, *J. Am. Chem. Soc.*, 2013, **135**, 7660.

19 T. Islamoglu, D. Ray, P. Li, M. B. Majewski, I. Akpinar, X. Zhang, C. J. Cramer, L. Gagliardi and O. K. Farha, From Transition Metals to Lanthanides to Actinides: Metal-Mediated Tuning of Electronic Properties of Isostructural Metal-Organic Frameworks, *Inorg. Chem.*, 2018, **57**, 13246.

20 O. A. Ejegbavwo, C. R. Martin, O. A. Olorunfemi, G. A. Leith, R. T. Ly, A. M. Rice, E. A. Dolgopolova, M. D. Smith, S. G. Karakalos, N. Birkner, B. A. Powell, S. Pandey, R. J. Koch, S. T. Misture, H. C. Zur Loye, S. R. Phillpot, K. S. Brinkman and N. B. Shustova, Thermodynamics and Electronic Properties of Heterometallic Multinuclear Actinide-Containing Metal-Organic Frameworks with 'structural Memory', *J. Am. Chem. Soc.*, 2019, **141**, 11628.

21 H. Xu, C.-S. Cao, X.-M. Kang and B. Zhao, Lanthanide-based metal–organic frameworks as luminescent probes, *Dalton Trans.*, 2016, **45**, 18003.

22 M. L. Mortensen, S. Bisht, M. Abbas, H. Firouzi, G. T. McCandless, M. Shatruk and K. J. Balkus, Lanthanide Metal–Organic Frameworks Exhibiting Fluoro-Bridged Extended Chains: Synthesis, Crystal Structures, and Magnetic Properties, *Inorg. Chem.*, 2024, **63**, 219, DOI: **10.1021/acs.inorgchem.3c03064**.

23 N. Panagiotou, F. G. Moscoso, T. Lopes-Costa, J. M. Pedrosa and A. J. Tasiopoulos, 2-Dimensional rare earth metal-organic frameworks based on a hexanuclear secondary building unit as efficient detectors for vapours of nitroaromatics and volatile organic compounds, *Inorg. Chem. Front.*, 2022, **9**, 4850.

24 J. P. Zhang, P. Q. Liao, H. L. Zhou, R. B. Lin and X. M. Chen, Single-crystal X-ray diffraction studies on structural transformations of porous coordination polymers, *Chem. Soc. Rev.*, 2014, **43**, 5789.

25 Y. Chen, K. B. Idrees, M. R. Mian, F. A. Son, C. Zhang, X. Wang and O. K. Farha, Reticular Design of Precise Linker Installation into a Zirconium Metal-Organic Framework to Reinforce Hydrolytic Stability, *J. Am. Chem. Soc.*, 2023, **145**, 3055.

26 C. G. Efthymiou, E. J. Kyprianidou, C. J. Milios, M. J. Manos and A. J. Tasiopoulos, Flexible lanthanide MOFs as highly selective and reusable liquid MeOH sorbents, *J. Mater. Chem. A*, 2013, **1**, 5061.

27 A. Demessence and J. R. Long, Selective gas adsorption in the flexible metal-organic frameworks Cu(BDTri)L (L = DMF, DEF), *Chem. – Eur. J.*, 2010, **16**, 5902.

28 Q. Q. Li, H. Liu, T. T. Zheng, P. Liu, J. X. Song and Y. Y. Wang, The effect of coordinated solvent molecules on metal coordination environments in single-crystal-to-single-crystal transformations, *CrystEngComm*, 2020, **22**, 6750.

29 E. Papazoi, A. Douvali, S. Rapti, E. Skliri, G. S. Armatas, G. S. Papaefstathiou, X. Wang, Z. F. Huang, S. Kaziannis, C. Kosmidis, A. G. Hatzidimitriou, T. Lazarides and M. J. Manos, A microporous Mg^{2+} MOF with cation exchange properties in a single-crystal-to-single-crystal fashion, *Inorg. Chem. Front.*, 2017, **4**, 530.

30 M. I. Gonzalez, A. B. Turkiewicz, L. E. Darago, J. Oktawiec, K. Bustillo, F. Grandjean, G. J. Long and J. R. Long, Confinement of atomically defined metal halide sheets in a metal–organic framework, *Nature*, 2020, **577**, 64.

31 S. Yuan, J. S. Qin, J. Su, B. Li, J. Li, W. Chen, H. F. Drake, P. Zhang, D. Yuan, J. Zuo and H. C. Zhou, Sequential Transformation of Zirconium(IV)-MOFs into Heterobimetallic MOFs Bearing Magnetic Anisotropic Cobalt(II) Centers, *Angew. Chem., Int. Ed.*, 2018, **57**, 12578.

32 L. F. Wang, W. M. Zhuang, G. Z. Huang, Y. C. Chen, J. Z. Qiu, Z. P. Ni and M. L. Tong, Spin-crossover modulation: Via single-crystal to single-crystal photochemical [2 + 2] reaction in Hofmann-type frameworks, *Chem. Sci.*, 2019, **10**, 7496.

33 M. I. Gonzalez, E. D. Bloch, J. A. Mason, S. J. Teat and J. R. Long, Single-crystal-to-single-crystal metalation of a metal-organic framework: A route toward structurally well-defined catalysts, *Inorg. Chem.*, 2015, **54**, 2995.

34 S. Yuan, L. Zou, H. Li, Y. P. Chen, J. Qin, Q. Zhang, W. Lu, M. B. Hall and H. C. Zhou, Flexible Zirconium Metal-Organic Frameworks as Bioinspired Switchable Catalysts, *Angew. Chem., Int. Ed.*, 2016, **55**, 10776.

35 S. Yuan, Y. P. Chen, J. S. Qin, W. Lu, L. Zou, Q. Zhang, X. Wang, X. Sun and H. C. Zhou, Linker Installation: Engineering Pore Environment with Precisely Placed Functionalities in Zirconium MOFs, *J. Am. Chem. Soc.*, 2016, **138**, 8912.

36 E. J. Kyprianidou, T. Lazarides, S. Kaziannis, C. Kosmidis, G. Itskos, M. J. Manos and A. J. Tasiopoulos, Single crystal coordinating solvent exchange as a general method for the enhancement of the photoluminescence properties of lanthanide MOFs, *J. Mater. Chem. A*, 2014, **2**, 5258.

37 X. Z. Song, S. Y. Song, S. N. Zhao, Z. M. Hao, M. Zhu, X. Meng, L. L. Wu and H. J. Zhang, Single-Crystal-to-Single-Crystal Transformation of a Europium(III) Metal-Organic Framework Producing a Multi-responsive Luminescent Sensor, *Adv. Funct. Mater.*, 2014, **24**, 4034.

38 S. Yuan, W. Lu, Y. P. Chen, Q. Zhang, T. F. Liu, D. Feng, X. Wang, J. Qin and H. C. Zhou, Sequential linker installation: Precise placement of functional groups in multivariate metal-organic frameworks, *J. Am. Chem. Soc.*, 2015, **137**, 3177.

39 C. C. Cao, C. X. Chen, Z. W. Wei, Q. F. Qiu, N. X. Zhu, Y. Y. Xiong, J. J. Jiang, D. Wang and C. Y. Su, Catalysis through Dynamic Spacer Installation of Multivariate Functionalities in Metal-Organic Frameworks, *J. Am. Chem. Soc.*, 2019, **141**, 2589.

40 W. Lin, E. Ning, L. Yang, Y. Rao, S. Peng and Q. Li, Snapshots of Postsynthetic Modification in a Layered Metal-Organic Framework: Isometric Linker Exchange and Adaptive Linker Installation, *Inorg. Chem.*, 2021, **60**, 11756.

41 C. D. S. Brites, S. Balabhadra and L. D. Carlos, Lanthanide-Based Thermometers: At the Cutting-Edge of Luminescence Thermometry, *Adv. Opt. Mater.*, 2019, **7**, 1.

42 Y. Zhang, S. Yuan, G. Day, X. Wang, X. Yang and H. C. Zhou, Luminescent sensors based on metal-organic frameworks, *Coord. Chem. Rev.*, 2018, **354**, 28.

43 V. Trannoy, A. N. Carneiro Neto, C. D. S. Brites, L. D. Carlos and H. Serier-Brault, Engineering of Mixed Eu^{3+}/Tb^{3+} Metal-Organic Frameworks Luminescent Thermometers with Tunable Sensitivity, *Adv. Opt. Mater.*, 2021, **9**(1).

44 X. Rao, T. Song, J. Gao, Y. Cui, Y. Yang, C. Wu, B. Chen and G. Qian, A highly sensitive mixed lanthanide metal-organic framework self-calibrated luminescent thermometer, *J. Am. Chem. Soc.*, 2013, **135**, 15559.

45 J. W. Hu, X. Y. Wang, J. Xu, X. Y. Dong and C. Zhang, Hypersensitive ratiometric temperature sensing in a bimetallic lanthanide metal-organic framework, *J. Mater. Chem. C*, 2023, **11**, 14545.

46 T. Xia, W. Cao, L. Guan, J. Zhang, F. Jiang, L. Yu and Y. Wan, Three isostructural hexanuclear lanthanide-organic frameworks for sensitive luminescence temperature sensing over a wide range, *Dalton Trans.*, 2022, **51**, 5426.

47 T. Xia, J. Wang, K. Jiang, Y. Cui, Y. Yang and G. Qian, A Eu/Gd-mixed metal-organic framework for ultrasensitive physiological temperature sensing, *Chin. Chem. Lett.*, 2018, **29**, 861.

48 A. Kourtellaris, W. Lafargue-Dit-Hauret, F. Massuyeau, C. Latouche, A. J. Tasiopoulos and H. Serier-Brault, Tuning of Thermometric Performances of Mixed Eu–Tb Metal–Organic Frameworks through Single-Crystal Coordinating Solvent Exchange Reactions, *Adv. Opt. Mater.*, 2022, **10**, 2200484, DOI: **10.1002/adom.202200484**.

49 R. M. Abdelhameed, D. Ananias, A. M. S. Silva and J. Rocha, Luminescent Nanothermometers Obtained by Post-Synthetic Modification of Metal-Organic Framework MIL-68, *Eur. J. Inorg. Chem.*, 2019, 1354.

50 J. De Bellis, L. Bellucci, G. Bottaro, L. Labella, F. Marchetti, S. Samaritani, D. Belli Dell'Amico and L. Armelao, Single-crystal-to-single-crystal post-synthetic modifications of three-dimensional LOFs (Ln = Gd, Eu): A way to modulate their luminescence and thermometric properties, *Dalton Trans.*, 2020, **49**, 6030.

51 Y. Long, Y. Zheng, Y. Xia, L. Qu, Y. Yang, H. Xiang and X. Zhou, Nickel-Catalyzed Synthesis of an Aryl Nitrile via Aryl Exchange between an Aromatic Amide and a Simple Nitrile, *ACS Catal.*, 2022, **12**, 4688.

52 O. V. Dolomanov, A. J. Blake, N. R. Champness and M. Schröder, OLEX: New software for visualization and analysis of extended crystal structures, *J. Appl. Crystallogr.*, 2003, **36**, 1283.

53 G. Sheldrick, A short history of SHELX, *Acta Crystallogr., Sect. A: Found. Crystallogr.*, 2008, **64**, 112.

54 E. OxfordDiffraction, CrysAlis CCD and CrysAlis RED, version p171.38.46; Oxford Diffraction Ltd, Abingdon, Oxford, 2017.
55 L. J. Farrugia, WinGX suite for small-molecule single-crystal crystallography, *J. Appl. Crystallogr.*, 1999, **32**, 837.
56 K. Brandenburg, *DIAMOND*, 2014, *Version 3.2k*.
57 A. L. Spek, Single-crystal structure validation with the program PLATON, *J. Appl. Crystallogr.*, 2003, **36**, 7.
58 N. Panagiotou, I. Liatsou, A. Pournara, G. K. Angeli, R. M. Giappa, E. Tylianakis, M. J. Manos, G. E. Froudakis, P. N. Trikalitis, I. Pashalidis and A. J. Tasiopoulos, Water-stable 2-D Zr MOFs with exceptional UO_2^{2+} sorption capability, *J. Mater. Chem. A*, 2020, **8**, 1849.
59 N. Panagiotou, K. Evangelou, A. Psalti, N. Varnava, G. K. Angeli, P. N. Trikalitis, J. C. Plakatouras, T. Lazarides and A. J. Tasiopoulos, Improving the Cd^{2+}detection capability of a new anionic rare earth metal-organic framework based on a $[RE_6(\mu_3\text{-}OH)_8]^{10+}$secondary building unit: An ion-exchange approach towards more efficient sensors, *Mol. Syst. Des. Eng.*, 2020, **5**, 1077.
60 J. P. Vizuet, M. L. Mortensen, A. L. Lewis, M. A. Wunch, H. R. Firouzi, G. T. McCandless and K. J. Balkus, Fluoro-Bridged Clusters in Rare-Earth Metal–Organic Frameworks, *J. Am. Chem. Soc.*, 2021, **143**, 17995.
61 J. I. Deneff, L. E. S. Rohwer, K. S. Butler, N. R. Valdez, M. A. Rodriguez, T. S. Luk and D. F. Sava Gallis, Covert MOF-Based Photoluminescent Tags via Tunable Linker Energetics, *ACS Appl. Mater. Interfaces*, 2022, **14**, 3038.
62 E. Loukopoulos, G. K. Angeli, K. Kouvidis, C. Tsangarakis and P. N. Trikalitis, Accessing 14-Connected Nets: Continuous Breathing, Hydrophobic Rare-Earth Metal Organic Frameworks Based on 14-c Hexanuclear Clusters with High Affinity for Non-Polar Vapors, *ACS Appl. Mater. Interfaces*, 2022, **14**, 3038, DOI: **10.1021/acsami.2c05961**.
63 M. Abbas, S. Sheybani, M. L. Mortensen and K. J. Balkus, Fluoro-bridged rare-earth metal–organic frameworks, *Dalton Trans.*, 2024, **53**, 3445–3453, DOI: **10.1039/D3DT03814A**.
64 X. N. Hua, L. Qin, X. Z. Yan, L. Yu, Y. X. Xie and L. Han, Conformational diversity of flexible ligand in metal-organic frameworks controlled by size-matching mixed ligands, *J. Solid State Chem.*, 2015, **232**, 91.
65 Q. Li, D. X. Xue, Y. F. Zhang, Z. H. Zhang and Z. Gao, Syntheses, crystal structures and photoluminescence properties of five Cd/Zn–organic frameworks, *J. Mol. Struct.*, 2018, **1164**, 123.
66 M. Llunell, D. Casanova, J. Girera, P. Alemany and S. Alvarez, Univ. Barcelona, Spain, 2013.
67 V. Guillerm, Ł. J. Weseliński, Y. Belmabkhout, A. J. Cairns, V. D'Elia, Ł. Wojtas, K. Adil and M. Eddaoudi, Discovery and introduction of a (3,18)-connected net as an ideal blueprint for the design of metal-organic frameworks, *Nat. Chem.*, 2014, **6**, 673.
68 C. Liu, S. V. Eliseeva, T. Y. Luo, P. F. Muldoon, S. Petoud and N. L. Rosi, Near infrared excitation and emission in rare earth MOFs: Via encapsulation of organic dyes, *Chem. Sci.*, 2018, **9**, 8099.
69 R. G. Abdulhalim, P. M. Bhatt, Y. Belmabkhout, A. Shkurenko, K. Adil, L. J. Barbour and M. Eddaoudi, A Fine-Tuned Metal-Organic Framework for Autonomous Indoor Moisture Control, *J. Am. Chem. Soc.*, 2017, **139**, 10715.
70 L. Feng, Y. Wang, K. Zhang, K. Y. Wang, W. Fan, X. Wang, J. A. Powell, B. Guo, F. Dai, L. Zhang, R. Wang, D. Sun and H. C. Zhou, Molecular Pivot-Hinge Installation to Evolve Topology in Rare-Earth Metal–Organic Frameworks, *Angew. Chem., Int. Ed.*, 2019, **58**, 16682.
71 G. K. Angeli, E. Loukopoulos, K. Kouvidis, A. Bosveli, C. Tsangarakis, E. Tylianakis, G. Froudakis and P. N. Trikalitis, Continuous Breathing Rare-Earth MOFs Based on Hexanuclear Clusters with Gas Trapping Properties, *J. Am. Chem. Soc.*, 2021, **143**, 10250.
72 Y. Wang, L. Feng, W. Fan, K. Y. Wang, X. Wang, X. Wang, K. Zhang, X. Zhang, F. Dai, D. Sun and H. C. Zhou, Topology Exploration in Highly Connected Rare-Earth Metal-Organic Frameworks via Continuous Hindrance Control, *J. Am. Chem. Soc.*, 2019, **141**, 6967.
73 X. P. Wang, W. M. Chen, H. Qi, X. Y. Li, C. Rajnák, Z. Y. Feng, M. Kurmoo, R. Boča, C. J. Jia, C. H. Tung and D. Sun, Solvent-Controlled Phase Transition of a CoII-Organic Framework: From Achiral to Chiral and Two to Three Dimensions, *Chem. – Eur. J.*, 2017, **23**, 7990.
74 B. Guo, H. Liu, J. Pang, Q. Lyu, Y. Wang, W. Fan, X. Lu and D. Sun, Tunable rare-earth metal−organic frameworks for ultra-high selenite capture, *J. Hazard. Mater.*, 2022, **436**, 129094.
75 M. Latvaa, H. Takalob, V. M. Mukkala, C. Matachescuc, J. C. Rodriguez-ubisd, J. Kankarea, M. Latva, H. Takalob, V. M. Mukkala, C. Matachescu, J. C. Rodríguez-Ubis and J. Kankare, Correlation between the lowest triplet state energy level of the ligand and lanthanide(III) luminescence quantum yield, *J. Lumin.*, 1997, **75**, 149.
76 J. Rocha, C. D. S. Brites and L. D. Carlos, Lanthanide Organic Framework Luminescent Thermometers, *Chem. – Eur. J.*, 2016, **22**, 14782.
77 T. Xia, Z. Shao, X. Yan, M. Liu, L. Yu, Y. Wan, D. Chang, J. Zhang and D. Zhao, Tailoring the triplet level of isomorphic Eu/Tb mixed MOFs for sensitive temperature sensing, *Chem. Commun.*, 2021, **57**, 3143.
78 C. D. S. Brites, A. Millán and L. D. Carlos, *Handbook on the Physics and Chemistry of Rare Earths*, 2016, **49**, 339.
79 C. D. S. Brites, P. P. Lima, N. J. O. Silva, A. Millán, V. S. Amaral, F. Palacio and L. D. Carlos, Lanthanide-based luminescent molecular thermometers, *New J. Chem.*, 2011, **35**, 1177.
80 M. D. Dramicanin, Trends in luminescence thermometry, *J. Appl. Phys.*, 2020, **128**, 40902.

